

Hydrothermal synthesis and electrochemical properties of MnFe_2O_4 nanoplates

Hanfeng Liang, Xun Xu, Jinqing Hong, Zhoucheng Wang*

Department of Chemical and Biochemical Engineering, College of Chemistry and Chemical Engineering, Xiamen University, 422 Siming South Road, Xiamen, 361000, China

*Corresponding author. Tel: (+86) 18059217473; Fax: (+46) 5912180738; E-mail: zcwang@xmu.edu.cn

Received: 06 December 2016, Revised: 10 March 2017 and Accepted: 07 April 2017

DOI: 10.5185/amlett.2017.1543

www.vbripress.com/aml

Abstract

MnFe_2O_4 nanoplates have been synthesized by a simple hydrothermal method. X-ray diffraction (XRD), Fourier transform infrared spectroscopy (FTIR), transmission electron microscopy (TEM), and selected area electron diffraction (SAED) have been employed to characterize the structure and morphology of the as-prepared sample. The results show that the products are plate-like morphology with 100-500 nm in length and 100-200 nm in thickness. Contrast experiments indicate that the formation of the plate-like nanostructure could be ascribed to the effect of citrate complexation. Magnetic measurements at 300 K gave the saturation magnetization and the coercive field of nanoplates 39.2 emu g^{-1} and 91.5 Oe, respectively. The electrochemical performance as anode material for lithium-ion batteries was further evaluated by cyclic voltammetry (CV), electrochemical impedance and charge-discharge measurements. It was demonstrated that the material could provide an initial reversible capacity of 1067 mAh g^{-1} at a current density of 0.1 mA cm^{-2} over the voltage range from 0.5 to 3.0 V. Copyright © 2017 VBRI Press.

Keywords: Magnetic materials, hydrothermal synthesis, formation mechanism, magnetic properties, electrochemical properties.

Introduction

Over the past decades, the synthesis and characterization of nanostructural magnetic materials have been attracting great interest because of their prospective novel magnetic properties with reduced dimensions [1]. MnFe_2O_4 , as one of the most important magnetic materials, has been widely used in many applications such as magnetic separation [2] and magnetic resonance imaging (MRI) [3] and catalysis [4] due to its high magnetic permeability and high electrical resistance. Considerable effort has been devoted to the design and controlled fabrication of magnetic nanomaterials with controlled size and shape. Various synthetic methods, such as template method [5], vapor growth [6], hydrothermal synthesis [7] and electrochemical deposition [8], and so on, are continually being improved to this end. Among all of these methods, the hydrothermal method, which can initiate the nucleation in the growth of nanocrystals, and promote the formation of crystalline products to completion under non-equilibrium conditions, has opened a new and promising path in controlling the morphology of particles [9]. To date, MnFe_2O_4 nanostructures with different morphologies, such as nanoparticles [2,10], rods [11], wires [12], fibers [13] and octahedrons [14] have been successfully synthesized.

However, most of these structures are one-dimensional or three-dimensional structures.

Two-dimensional (2-D) nanomaterials are an interesting class of materials whose surface area is dominated by one specific crystallographic plane; therefore they are almost crystallographically isotropic. As one of the two-dimensional materials, nanoplates have received intensive research due to their potential applications in electronics, energy storage and catalysis. Some metal oxides in plate-like shape, such as ZnO [15], MnO_2 [16], CuO [17], and Bi_2WO_6 [18] have been applied as anode materials for lithium ion batteries (LIBs). The initial discharge capacities of these materials usually exceed 1000 mAh g^{-1} (that is, about three times those of commonly used graphite) [19]. However, it is commonly challengeable to build up an integrated smart architecture using a simple and facile approach, in which structural features and electroactivities of each component are fully manifested, and the interface/chemical distributions are homogeneous at the nanoscale. Therefore, the energy density of LIBs can be promoted by utilizing the mixed transition metal oxides nanoplates as anode materials. However, to the best of our knowledge, there has not been any report on the fabrication of MnFe_2O_4 nanoplates as anode materials. Herein, we present a simple hydrothermal route to synthesis of MnFe_2O_4 nanoplates. The morphological details and

possible formation mechanism of the as-prepared nanoplates were investigated in detail. The as-prepared MnFe_2O_4 delivered an initial specific capacity as high as 1067 mAh g^{-1} at a current density of 0.1 mA cm^{-2} over the voltage range from 0.5 to 3.0 V, which showed superior capacity and low potential window than graphite [19]. It was found that the sodium citrate and NaOH play key roles in the formation of the MnFe_2O_4 nanoplates.

Experimental

Material synthesis

In a typical experiment, 1.5 mmol of $(\text{NH}_4)_2\text{Fe}(\text{SO}_4)_2 \cdot 6\text{H}_2\text{O}$, 0.75 mmol of $\text{MnCl}_2 \cdot 4\text{H}_2\text{O}$ and 3 mmol of sodium citrate were dissolved in 20 mL of deionized water under stirring. Subsequently, 20 mL NaOH aqueous were introduced into the above homogeneous solution. The final concentration of NaOH in solution is 0.625 M. The whole mixture was stirred for another 30 min and then transferred into a Teflon-lined stainless steel autoclave of 50 mL capacity, sealed and maintained at $180 \text{ }^\circ\text{C}$ for 24 h. When the reactions were completed, the autoclave was cooled to room temperature naturally. The products were filtered and washed several times with distilled water and absolute ethanol, and finally dried in a vacuum oven at $60 \text{ }^\circ\text{C}$ for 12 h.

Characterizations

The phase purity of the product was examined by X-ray powder diffraction (XRD) using an X'pert PRO X-ray diffractometer at a voltage of 40 kV and a current of 30 mA with Cu K α radiation ($\lambda=1.54\text{\AA}$). Fourier transform infrared (FTIR) spectra were recorded on a Nicolet 380 spectrometer. Field emission scanning electron microscopy (FESEM) images were obtained using a LEO 1530 microscope (Germany). Transmission electron microscopy (TEM) images and the corresponding selected area electron diffraction (SAED) pattern were taken on a JEOL JEM-2100 transmission electron microscope at an accelerating voltage of 200 kV. Magnetic measurements were carried out at room temperature using a SQUID magnetometer (Quantum Design MPMS-XL-7) with a maximum magnetic field of 15 kOe.

Electrochemical Measurements

The MnFe_2O_4 electrodes were prepared by drying a slurry (composed of 85 wt% active material, 10 wt% carbon black, and 5 wt% polyvinylidene fluoride dissolved in N-methyl-2-pyrrolidone) on an Al foil at $120 \text{ }^\circ\text{C}$ for 2 h. CR2025-type coin cells were assembled in a glove box for electrochemical characterization. A lithium metal sheet was used as the counter electrode, while the electrolyte was 1M LiPF_6 in a mixture of ethylene carbonate, dimethyl carbonate and methyl ethyl carbonate (1:1:1 by volume). The cells were galvanostatically charged and discharged at a current density of 0.2 mA cm^{-2} within the range of 0.5-3.0 V. Cyclic voltammetry (CV)

curves were collected at 2 mV s^{-1} within the range of 2.0-4.5 V. In the electrochemical impedance spectroscopy (EIS) measurement, the excitation voltage applied to the cells was 5 mV and the frequency range was between 100 kHz and 10 mHz. Both the CV and EIS measurements were carried out on an electrochemistry workstation (CHI660C).

Results and discussion

Fig. 1a shows the XRD pattern of the as-prepared product. The XRD diffraction patterns of synthesized material show the reflection planes (111), (220), (311), (400), (422), (511), (440), (622) which confirm the presence of single-phase in MnFe_2O_4 . All the diffraction peaks can be indexed to a cubic spinelle phase with the lattice constants of $a = b = c = 8.499 \text{ \AA}$ (space group: Fd-3m), which are consistent with the values in the literature (JCPDS no. 88-1965). No characteristic peaks from other phases were detected, indicating the high purity of the product. **Fig. 1b** shows the FTIR spectrum of the MnFe_2O_4 nanoplates. The vibration band with peaks at 572 cm^{-1} and 469 cm^{-1} in the spectrum can be assigned to the stretching modes of Fe-O and Mn-O bond. The other two bands at 1600 and 3390 cm^{-1} were due to the stretching vibration of -OH and bending vibration of the H_2O molecules, respectively [20].

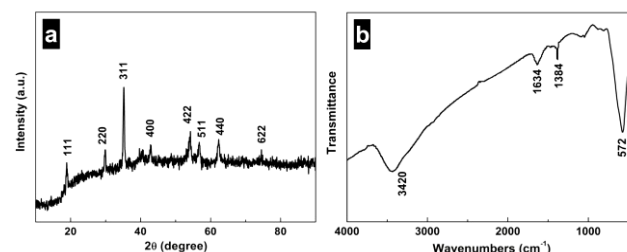


Fig. 1 (a) XRD pattern and, (b) FTIR spectrum of the as-prepared MnFe_2O_4 nanoplates.

The size and morphology of the product were examined by FESEM and TEM measurements. The FESEM image in **Fig. 2a** shows the general morphology of the MnFe_2O_4 nanoplates synthesized in this work. It can be found that the MnFe_2O_4 sample consisted of almost entirely of nanoplates, indicating the high-yield growth and good uniformity of the product. **Fig. 2b** presents a high magnification FESEM image of nanoplates, which clearly reveals these nanoplates are 100-500 nm in length and 100-200 nm in thickness. The morphology and structure details of the as-prepared sample were further detected by TEM and SAED. **Fig. 2c** displays a typical TEM image of these plates, showing the same morphological characteristic with that of FESEM observations. Some nanoplates were stacked, which were viewed edgewise (**Fig. 2d**). From the image of one individual MnFe_2O_4 nanoplate shown in **Fig. 2e**, the plate-like morphology and rough surface can be seen clearly, which agrees with the FESEM result. The inset is the corresponding SAED pattern, which is consistent with the XRD result.

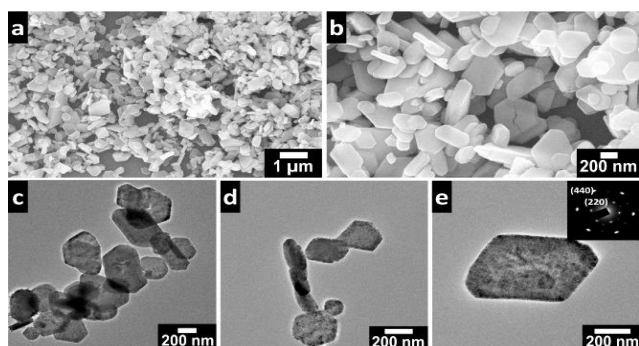


Fig. 2 Morphological images of the as-prepared sample: (a, b) FESEM images and (c, d, e) TEM images. The inset of panel e is the corresponding SAED pattern.

In our synthetic route, sodium citrate played a key role in the formation of MnFe_2O_4 nanoplates. For the controlled experiment for the absence of sodium citrate, only irregular shapes were obtained in hydrothermal process (**Fig. 3a**). In the contrast, if sodium citrate were introduced into the solution, the MnFe_2O_4 nanoplates could be synthesised. In addition, the plate-like structures can be obtained in the presence of either citrate yet cannot be obtained in the presence of KCl or NaCl solely. This indicates that the citrate anions are essential for the formation of the plate-like structures. As we know, citrate is an important biological ligand for metal ions. It can form strong complexes with Ni^{2+} , Co^{2+} , Fe^{3+} , Zn^{2+} , and Ag^+ ions [21]. In this system, the chelation of citrate with metal ions decreases the free $\text{Fe}^{3+}/\text{Mn}^{2+}$ concentration in solution and results in the slow generation of MnFe_2O_4 nanoplates. The relatively slow reaction was favorable for separating the growth step from the nucleation step and responsible for the oriented growth [22]. Meanwhile, citrate can also serve as a shape modifier and controller. The stereochemical characteristics of citrate molecules lead to multiple binding sites for the three carboxylic acid groups when interacting with crystal surfaces. Thus, the citrate may bind to certain crystal faces of the MnFe_2O_4 particles through its acetate functions. This can be confirmed by the FTIR spectroscopic evidence on the presence of bond at 1384 cm^{-1} , which was attributed to acetate bending vibration of the citrate complexed with metal ions. It is clear that the adsorption of citrate will inevitably depend on the surface density of metal atoms. Thus, the face with a higher density of surface atoms is blocked by the adsorption of citrate during the growth of nanocrystals, and the growth along this facet is therefore considerably restricted, which means that the nuclei grow in a two-dimensional mode to produce nanoplates [23].

In order to investigate how NaOH concentration affects the morphology of MnFe_2O_4 nanostructures during a hydrothermal process, we have performed experiments with NaOH concentrations of 0.5, 0.625, 0.75, 1.25 and 2.5 M, respectively, keeping other reaction conditions unchanged. It is found that it is necessary for the formation of plate-like MnFe_2O_4 nanostructures that a sufficient amount of NaOH was used as well as the addition of citrate. **Fig. 3b-f** show the SEM images of the

samples obtained after hydrothermal reaction with different concentrations of NaOH. **Fig. 3b, d, and f** show that MnFe_2O_4 nanostructures prepared with 0.5, 0.75, and 2.5 M NaOH, respectively, are composed of nanoplates with large length and particles. When the experiment is carried out with NaOH concentration of 0.625 M, nanoplates are obtained as shown in **Fig. 3c**. When NaOH concentration increases to 1.25 M, the product is composed of farinose particles as shown in **Fig. 3e**. It can be found that with increase of the concentration of NaOH, the composition of MnFe_2O_4 nanostructures changed seems like a cycle: plates and particles \rightarrow plates \rightarrow plates and particles \rightarrow particles \rightarrow plates and particles. It has been reported that the solubility of nanoparticles with high defects can be increased greatly in solution with high NaOH concentration [24]. Our experimental results demonstrate that NaOH can dissolve the nanoplates to form nanoparticles. While at an appropriate NaOH concentration, the dissolved nanoparticles grew into nanoplates through recrystallization process.

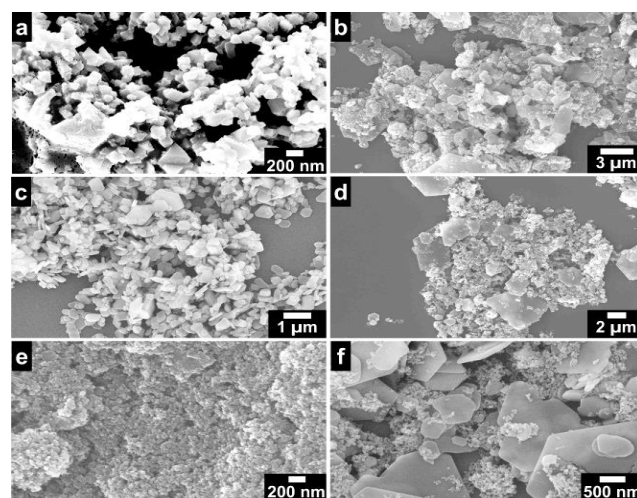


Fig. 3 FESEM images of the samples obtained after hydrothermal reaction (a) without sodium citrate and (b-f) with different concentrations of NaOH. (b) $C[\text{NaOH}] = 0.5\text{ M}$, (c) $C[\text{NaOH}] = 0.625\text{ M}$, (d) $C[\text{NaOH}] = 0.75\text{ M}$, (e) $C[\text{NaOH}] = 1.25\text{ M}$, and (f) $C[\text{NaOH}] = 2.5\text{ M}$.

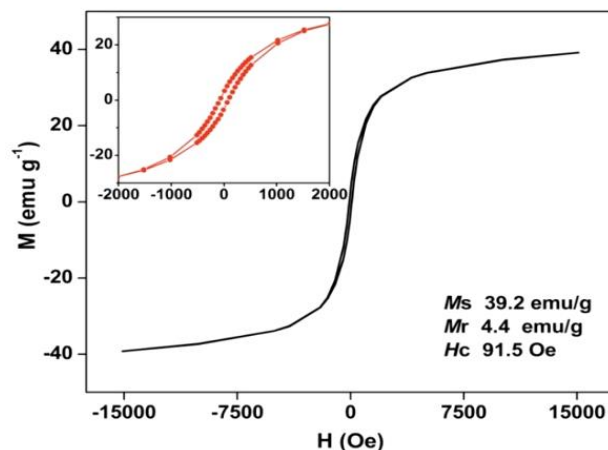


Fig. 4 Hysteresis loop of the as-prepared sample at room temperature.

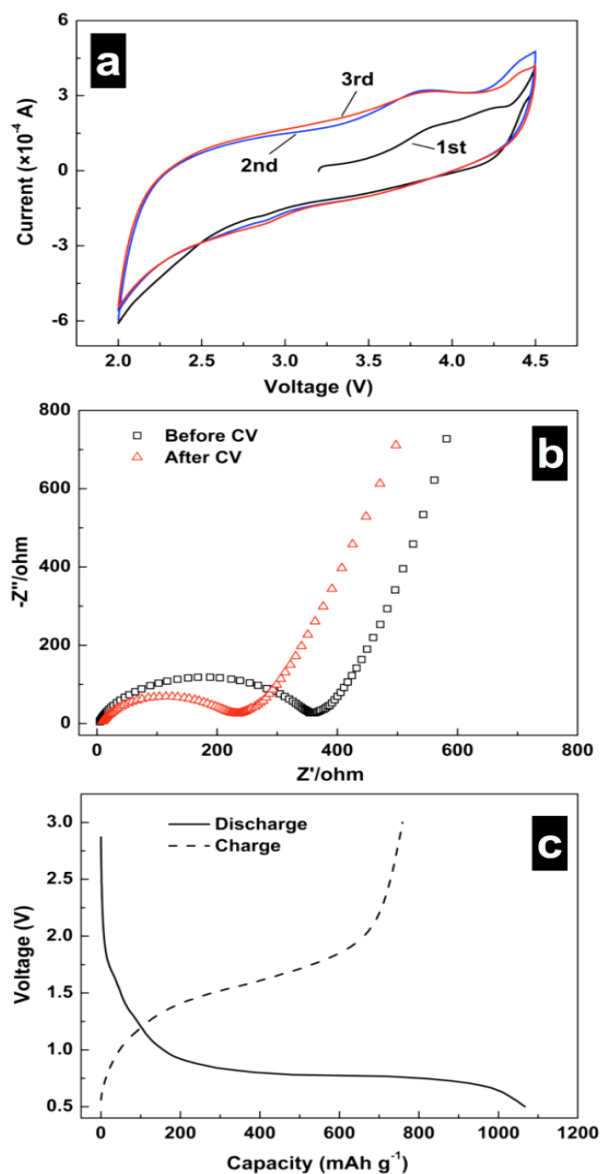


Fig. 5 Electrochemical measurements of the sample. (a) CVs between 2.0 V and 4.5 V at a scan rate of 2 mV s⁻¹. (b) Nyquist plots in the open circuit voltage. (c) Charge-discharge profiles for the first cycle at 0.2 mA cm⁻².

Fig. 4 shows the magnetic hysteresis curve for the MnFe₂O₄ nanoplates measured at room temperature in an applied magnetic field sweeping from -15 to 15 KOe. The hysteresis loop of the MnFe₂O₄ sample exhibits a weak ferromagnetic behavior with saturation magnetization (M_s), remanent magnetization (M_r), and coercivity (H_c) values of 39.2 emu g⁻¹, 4.4 emu g⁻¹, and 91.5 Oe, respectively. The values are different from those reported for MnFe₂O₄ nanorods ($M_s = 68.02$, $M_r = 14$ emu g⁻¹, $H_c = 361$ Oe) [14] and octahedrons ($M_s = 67$, $M_r = 26$ emu g⁻¹, $H_c = 520$ Oe) [14]. The lower saturation magnetization of nanoplates may be attributed to the surface effects with small particle size, and the lower coercivity value may be due to the magnetic flux closure vortex states in MnFe₂O₄ nanoparticles. **Fig. 5a** shows the cyclic voltammograms of the as-prepared MnFe₂O₄ nanoplates. The profile is close to rectangular shape, which exhibits a capacitive

performance in the potential window of 2.0-4.5 V. This result is completely different from those of the previously reported ferrite compounds, such as CoFe₂O₄ [25], which shows obvious peaks of redox reaction pairs. **Fig. 5b** presents typical Nyquist plots obtained before and after the CV experiments on the same electrode. The plots are similar to each other in shape, with a semicircle appearing in the high frequency domain and a straight line in the low frequency region. The numerical value of the diameter of the semicircle on the Z_{re} axis gives an approximate indication of the charge transfer resistance (R_{ct}). Before the CV experiments, the semicircle is about 360 Ω in terms of resistance, while the semicircle become smaller and the resistance value decreases to about 240 Ω after the CV experiments, which indicates that the charge transfer at the electrode-electrolyte interface is easier process after the CV cycles. When MnFe₂O₄ is charged and discharged between 0.5 and 3.0 V, as shown in **Fig. 5c**, MnFe₂O₄ has enough low potential to be used as an anode material for lithium ion batteries and much higher capacity than graphite, the commercial anode material [19]. The discharge profile shows an extended flat voltage profile around 0.75 V. The sample delivered a large discharge capacity of 1067 mAh g⁻¹ at 0.1 mA cm⁻², corresponding to the lithium uptake of about 9.2 Li per MnFe₂O₄. As we know, the maximum uptake of 8 Li per formula unit can be obtained by complete reduction of Mn²⁺ to Mn⁰ and Fe³⁺ to Fe⁰. Therefore, the theoretical discharge capacity is about 933 mAh g⁻¹ per mol MnFe₂O₄. The phenomenon that the first discharge capacity considerably exceeds the theoretical capacity has been widely reported for transition metal oxides [26-28]. The extra capacity beyond the theoretical value is probably due to the decomposition of non-aqueous electrolyte at low operating voltage and the subsequent formation of an organic layer on the surface of the electrode.

Conclusion

In summary, MnFe₂O₄ nanoplates have been successfully synthesized by a facile hydrothermal method. It is found that the sodium citrate and NaOH play critical roles in the formation of such plate-like structures. The as-synthesized sample exhibits a weak ferromagnetic property at room temperature with a coercive force of 91.5 Oe and a remnant magnetization of 4.4 emu g⁻¹. The electrochemical properties were also investigated. The material as-prepared shows superior electrochemical performance, with a high initial capacity of 1067 mAh g⁻¹, which makes the MnFe₂O₄ nanoplates a promising anode material for high-performance lithium-ion batteries.

Acknowledgements

The authors would like to thank the National Natural Science Foundation of China (51372212).

Author's contributions

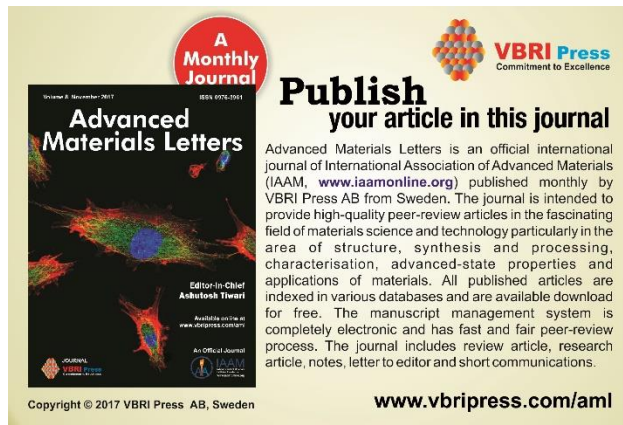
Conceived the plan: zcw; Performed the experiments: hfl, jqh; Data analysis: xx, hfl; Wrote the paper: hfl, zcw. Authors have no competing financial interests.

Supporting information

Supporting informations are available from VBRI Press.

References

1. Leslie-Pelecky, D.L.; Rieke, R.D.; *Chem. Mater.*, **1996**, *8*, 1770-1783.
DOI: [10.1021/cm960077f](https://doi.org/10.1021/cm960077f)
2. Mou, F.; Pan, D.; Chen, C.; Gao, Y.; Xu, L.; Guan, J.; *Adv. Funct. Mater.*, **2015**, *25*, 6173-6181.
DOI: [10.1002/adfm.201502835](https://doi.org/10.1002/adfm.201502835)
3. Kanagesan, S.; Hashim, M.; Aziz, S.A.B.; Ismail, I.; Tamilselvan, S.; Alitheen, N.B.; Swamy, M.K.; Rao, B.P.C.; *Molecules*, **2016**, *21*, 312.
DOI: [10.3390/molecules21030312](https://doi.org/10.3390/molecules21030312)
4. Zhou, Y.; Xiao, B.; Liu, S.; Meng, Z.; Chen, Z.; Zou, C.; Liu, C.; Chen, F.; Zhou, X.; *Chem. Eng. J.*, **2016**, *283*, 266-275.
DOI: [10.1016/j.cej.2015.07.049](https://doi.org/10.1016/j.cej.2015.07.049)
5. Mlondo, S.N.; Andrews, E.M.; Thomas, P.J.; Brien, P. O.; *Chem. Commun.*, **2008**, *24*, 2768-2770.
DOI: [10.1039/B806409A](https://doi.org/10.1039/B806409A)
6. Lao, J.Y.; Wen, J.G.; Ren, Z.F.; *Nano Lett.*, **2002**, *2*, 1287-1291.
DOI: [10.1021/nl025753t](https://doi.org/10.1021/nl025753t)
7. Wang, W.; Ding, Z.; Cai, M.; Jian, H.; Zeng, Z.; Li, F.; Ping J.; *Appl. Surf. Sci.*, **2015**, *346*, 348-353.
DOI: [10.1016/j.apsusc.2015.04.031](https://doi.org/10.1016/j.apsusc.2015.04.031)
8. Han, X.; Zhou, S.; Fan, H.; Zhang, Q.; Liu, Y.; *J Electroanal. Chem.*, **2015**, *755*, 203-209.
DOI: [10.1016/j.jelechem.2015.07.054](https://doi.org/10.1016/j.jelechem.2015.07.054)
9. Siskin M.; Katritzky, A. R.; *Chem. Rev.*, **2001**, *101*, 825-836.
DOI: [10.1021/cr000088z](https://doi.org/10.1021/cr000088z)
10. Xiao, Y.; Liang, H.; Chen, W.; Wang, Z.; *Appl. Sur. Sci.*, **2013**, *285*, 498-504.
DOI: [10.1016/j.apsusc.2013.08.083](https://doi.org/10.1016/j.apsusc.2013.08.083)
11. Hosseini, S.H.; Asadnia, A.; *Int. J. Phys. Sci.*, **2013**, *8*, 1209-1217.
DOI: [10.5897/IJPS12.576](https://doi.org/10.5897/IJPS12.576)
12. Malkinski, L.; Lim, J.H.; Chae, W.S.; Lee, H.O.; Kim, E.M.; Jung, J.S.; *Electron. Mater. Lett.*, **2009**, *5*, 87-90.
DOI: [10.3365/eml.2009.06.087](https://doi.org/10.3365/eml.2009.06.087)
13. Ju, Y.; Park, J.; Jung, H.; Cho, S.; Lee, W.; *Compos. Sci. Technol.*, **2008**, *68*, 1704-1709.
DOI: [10.1016/j.compscitech.2008.02.015](https://doi.org/10.1016/j.compscitech.2008.02.015)
14. Zhang, D.; Zhang, X.; Ni, X.; Song, J.M.; Zheng, H.; *Chem. Phys. Lett.*, **2006**, *426*, 120-123.
DOI: [10.1016/j.cplett.2006.05.100](https://doi.org/10.1016/j.cplett.2006.05.100)
15. Gao, S.; Li, H.; Yuan, J.; Li, Y.; Yang, X.; Liu, J.W.; *Appl. Sur. Sci.*, **2010**, *256*, 2781-2785.
DOI: [10.1016/j.apsusc.2009.11.028](https://doi.org/10.1016/j.apsusc.2009.11.028)
16. Kim, J.; Kim, J. S.; Baik, H.; Kang, K.; Lee, K.; *RSC Adv.*, **2016**, *6*, 26535-26539.
DOI: [10.1039/C6RA01091A](https://doi.org/10.1039/C6RA01091A)
17. Beitollahi, H.; Ivari, S.G.; Torkzadeh-Mahani, M.; *Mater. Sci. Eng. C*, **2016**, *69*, 128-133.
DOI: [10.1016/j.msec.2016.06.064](https://doi.org/10.1016/j.msec.2016.06.064)
18. Xu, X.; Ming, F.; Hong, J.; Xie, Y.; Wang, Z.; *Mater. Lett.*, **2016**, *179*, 52-56.
DOI: [10.1016/j.matlet.2016.05.031](https://doi.org/10.1016/j.matlet.2016.05.031)
19. Taberna, P. L.; Mitra, S.; Poizot, P.; Simon, P.; Tarascon, J. M.; *Nat. Mater.*, **2006**, *5*, 567-573.
DOI: [10.1038/nmat1672](https://doi.org/10.1038/nmat1672)
20. Jitianu, A.; Crisan, M.; Meghea, A.; Rau, I.; Zaharescu, M.; *J. Mater. Chem.*, **2002**, *12*, 1401-1407.
DOI: [10.1039/B110652J](https://doi.org/10.1039/B110652J)
21. Parkinson, J.A.; Sun, H.Z.; *Chem. Commun.*, **1998**, *8*, 881-882.
DOI: [10.1039/A708710A](https://doi.org/10.1039/A708710A)
22. Liang, J.; Liu, J.; Xie, Q.; Bai, S.; Yu, W.; Qian, Y.; *J. Phys. Chem. B* **2005**, *109*, 9463-9467.
DOI: [10.1021/jp050485j](https://doi.org/10.1021/jp050485j)
23. Si, R.; Zhang, Y.W.; You, L.P.; Yan, C.H.; *Angew. Chem, Int. Ed.*, **2005**, *44*, 3256-3260.
DOI: [10.1002/ange.200462573](https://doi.org/10.1002/ange.200462573)
24. Wang, Y.; Cheng, R.; Wen, Z.; Zhao, L.; *Eur. J. Inorg. Chem.*, **2011**, 2942-2947.
DOI: [10.1002/ejic.201100205](https://doi.org/10.1002/ejic.201100205)
25. Chu, Y.Q.; Fu, Z.W.; Qin, Q.Z.; *Electrochim. Acta.*, **2004**, *49*, 4915-4921.
DOI: [10.1016/j.electacta.2004.06.012](https://doi.org/10.1016/j.electacta.2004.06.012)
26. Hang, B.T.; Doi, T.; Okada, S.; Yamaki, J.-i.; *J. Power Sources*, **2007**, *174*, 493-500.
DOI: [10.1016/j.jpowsour.2007.06.031](https://doi.org/10.1016/j.jpowsour.2007.06.031)
27. Morimoto, H.; Tobishima, S.-i.; Iizuka Y.; *J. Power Sources*, **2005**, *146*, 315-318.
DOI: [10.1016/j.jpowsour.2005.03.036](https://doi.org/10.1016/j.jpowsour.2005.03.036)
28. Liu, S.; Zhang, L.; Zhou, J.; Xiang, J.; Sun, J.; Guan, J.; *Chem. Mater.*, **2008**, *20*, 3623-3628.
DOI: [10.1021/cm703623v](https://doi.org/10.1021/cm703623v)



A Monthly Journal

Publish your article in this journal

Advanced Materials Letters is an official international journal of International Association of Advanced Materials (IAAM, www.iaamonline.org) published monthly by VBRI Press AB from Sweden. The journal is intended to provide high-quality peer-review articles in the fascinating field of materials science and technology particularly in the area of structure, synthesis and processing, characterisation, advanced-state properties and applications of materials. All published articles are indexed in various databases and are available download for free. The manuscript management system is completely electronic and has fast and fair peer-review process. The journal includes review article, research article, notes, letter to editor and short communications.

Editor-in-Chief
Ashutosh Tiwari

Available on the e
www.dorpress.com/AM

An Official Journal
IAAM

Copyright © 2017 VBRI Press AB, Sweden

www.vbripress.com/aml

Supporting information**Table S1**

Comparison of anode material for lithium ion batteries.

Anode material	Potential window	Specific capacities	Ref.
CoO/CoFe ₂ O ₄ nanocomposites	0-3.0 V	1247 mAh g ⁻¹	Chem. Commun., 2012, 48, 410–412
NiFe ₂ O ₄ Nanofibers	0-3.5 V	870 mAh g ⁻¹	ACS Appl. Mater. Interfaces 2013, 5, 9957-9963
ZnCo ₂ O ₄ Nanowires	0-3.0 V	1197.9 mAh g ⁻¹	Inorg. Chem., 2011, 50, 3320-3324.
Fe ₃ O ₄ Sheath	0-3.0 V	800 mAh g ⁻¹	Nano Lett. 2013, 13, 818–823
MnFe ₂ O ₄	0.5-3.0 V	1067 mAh g ⁻¹	this work

Supporting Information

Table S1. Comparison of anode material for lithium ion batteries.

Anode material	Potential window	Specific capacities	Ref.
CoO/CoFe ₂ O ₄ nanocomposites	0-3.0 V	1247 mAh g ⁻¹	Chem. Commun., 2012, 48, 410–412
NiFe ₂ O ₄ Nanofibers	0-3.5 V	870 mAh g ⁻¹	ACS Appl. Mater. Interfaces 2013, 5, 9957-9963
ZnCo ₂ O ₄ Nanowires	0-3.0 V	1197.9 mAh g ⁻¹	Inorg. Chem., 2011, 50, 3320-3324.
Fe ₃ O ₄ Sheath	0-3.0 V	800 mAh g ⁻¹	Nano Lett. 2013, 13, 818–823
MnFe ₂ O ₄	0.5-3.0 V	1067 mAh g ⁻¹	this work